






## Approaching a thermal tipping point in the Eurasian boreal forest at its southern margin

Mukund Palat Rao <sup>1,2,3,4✉</sup>, Nicole K. Davi<sup>4,5</sup>, Troy S. Magney<sup>3</sup>, Laia Andreu-Hayles <sup>1,4,6</sup>, Baatarbileg Nachin<sup>4,7</sup>, Byambagerel Suran<sup>7,8</sup>, Arianna M. Varuolo-Clarke <sup>9,10</sup>, Benjamin I. Cook<sup>10,11</sup>, Rosanne D. D'Arrigo<sup>4</sup>, Neil Pederson <sup>4,12</sup>, Lkhagvajargal Odrentsen<sup>13</sup>, Milagros Rodríguez-Catón<sup>3,4</sup>, Caroline Leland<sup>4,5</sup>, Jargalan Burentogtokh<sup>14</sup>, William R. M. Gardner<sup>14</sup> & Kevin L. Griffin <sup>8,15,16</sup>

Climate change is increasing the intensity and frequency of extreme heat events. Ecological responses to extreme heat will depend on vegetation physiology and thermal tolerance. Here we report that *Larix sibirica*, a foundation species across boreal Eurasia, is vulnerable to extreme heat at its southern range margin due to its low thermal tolerance ( $T_{crit}$  of photosynthesis: ~37–48 °C). Projections from CMIP6 Earth System Models (ESMs) suggest that leaf temperatures might exceed the 25<sup>th</sup> percentile of *Larix sibirica*'s  $T_{crit}$  by two to three days per year within the next two to three decades (by 2050) under high emission scenarios (SSP3-7.0 and SSP5-8.5). This degree of warming will threaten the biome's continued ability to assimilate and sequester carbon. This work highlights that under high emission trajectories we may approach an abrupt ecological tipping point in southern boreal Eurasian forests substantially sooner than ESM estimates that do not consider plant thermal tolerance traits.

<sup>1</sup>CREAF, Cerdanyola del Valles, Barcelona, Spain. <sup>2</sup>Cooperative Programs for the Advancement of Earth System Science, University Corporation for Atmospheric Research, Boulder, CO, USA. <sup>3</sup>Department of Plant Sciences, University of California Davis, Davis, CA, USA. <sup>4</sup>Tree Ring Laboratory, Lamont-Doherty Earth Observatory of Columbia University, Palisades, NY, USA. <sup>5</sup>Department of Environmental Science, William Paterson University, Wayne, NJ, USA. <sup>6</sup>ICREA, Barcelona, Spain. <sup>7</sup>Institute of Forestry, National University of Mongolia, Ulaanbaatar, Mongolia. <sup>8</sup>Department of Environment and Forest Engineering, National University of Mongolia, Ulaanbaatar, Mongolia. <sup>9</sup>Department of Earth and Environmental Science, Columbia University, New York, NY, USA. <sup>10</sup>Ocean & Climate Physics, Lamont-Doherty Earth Observatory of Columbia University, Palisades, NY, USA. <sup>11</sup>NASA Goddard Institute for Space Studies, New York, NY, USA. <sup>12</sup>Harvard Forest, Harvard University, Petersham, MA, USA. <sup>13</sup>Graduate School, National University of Mongolia, Ulaanbaatar, Mongolia. <sup>14</sup>Department of Anthropology, Yale University, New Haven, CT, USA. <sup>15</sup>Biology & Paleoenvironment, Lamont-Doherty Earth Observatory of Columbia University, Palisades, NY, USA. <sup>16</sup>Ecology, Evolution, & Environmental Biology, Columbia University, New York, NY, USA. ✉email: [mukund24rao@gmail.com](mailto:mukund24rao@gmail.com)

The circumpolar boreal forest is the most extensive biome covering ~15 million km<sup>2</sup> and accounts for nearly a third of the 450Gt terrestrial carbon stock<sup>1–3</sup>. Boreal carbon resides in three major pools: peatlands, soils and forest biomass<sup>4</sup>. All pools are sensitive to rising temperatures from human-caused climate change due to direct impacts of warming and indirect impacts such as permafrost thaw, increased wildfire, and insect activity<sup>3–5</sup>. Two-thirds of the circumpolar boreal biome lies in Eurasia and North Mongolia, defined here as a ~1 million km<sup>2</sup> region between 95–114°E and 46–52°N, is located at the southern margin of the Eurasian boreal biome (Fig. 1a). The presence of boreal forest in North Mongolia can be attributed to its relatively cool mesic climate with mean annual precipitation generally exceeding 350 mm/year and mean annual temperatures between –5 and 0 °C (Fig. 1b and Supplementary Fig. 1a)<sup>6,7</sup>. Further south, the dominant ecosystem rapidly transitions into grassland-steppe due to warmer and drier climate conditions<sup>8</sup>.

Boreal regions can host stable but competing forest, shrub, and grassland-steppe ecosystems as a result of various land-atmosphere feedbacks such as albedo, fire, and insects<sup>6,7,9,10</sup>. Over the past four decades since the mid-1980s, accelerated warming and associated drying have decreased forest productivity and shifted the southern boreal forest margin northward, consistent with early stages of a projected ecosystem transition towards grass and shrublands<sup>11,12</sup>. Under continued global change, many Earth System Models (ESMs) predict the

exceedance of a ‘tipping point’ in the southern boreal forest, a critical threshold at which a small perturbation in forcing (e.g., temperature) can fundamentally and irreversibly alter the ecosystem state at regional to sub-continental spatial scales (order of several hundred kilometres) over human timescales<sup>13</sup>. ESMs forecast synchronised southern margin boreal forest dieback to commence at ~1.5 °C of global warming, become widespread by ~3.5 °C, and exceed a biome-wide tipping point at ~4 °C of global warming relative to 1850 C.E pre-industrial levels<sup>9</sup>. Upon crossing this tipping point, southern boreal forest dieback is projected to occur over ~50–100 year timescales and result in up to ~52GtC of potential emissions<sup>9,13</sup>. Notably, North Mongolia and the circumpolar boreal forest have already warmed three times faster than global temperature due to Arctic amplification<sup>10,14–18</sup> (Fig. 1c, d and Supplementary Fig. 2), with negative impacts on high-elevation Altai permafrost, tree growth<sup>19</sup>, and pastoral nomadic herding, the latter a traditional source of livelihood for a third of all Mongolians<sup>8,20–22</sup>. ESMs participating in the sixth phase of the Coupled Model Intercomparison Project (CMIP6<sup>23</sup>) suggest that warming will persist and intensify through the 21st century without compensating increases in precipitation (Fig. 1c, d and Supplementary Figs. 2, 3). Consequently, the North Mongolian boreal forest will increasingly be exposed to a higher temperature and temperature-related drought stress from enhanced net surface radiation as a result of inhibited longwave cooling and higher vapour pressure deficits<sup>24,25</sup>.

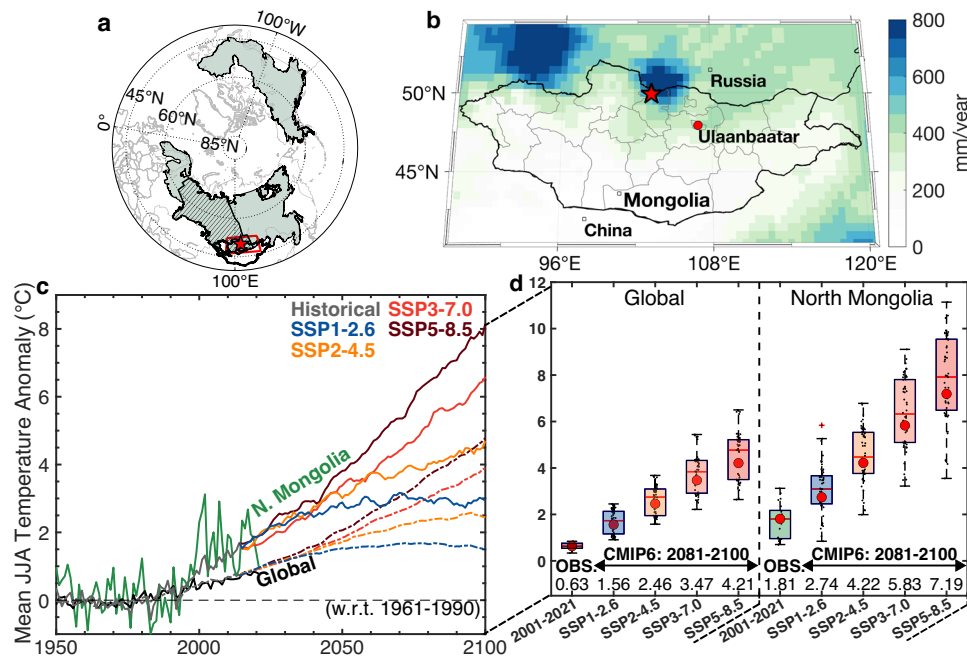


**Fig. 1** Climate trends and projections in North Mongolia and the globe. **a** Distribution of *Larix sibirica* (black hatching)<sup>44,46</sup> in the context of North Mongolia (red rectangle), our study site (103.17°E, 49.92°N, red star), and the circumpolar boreal biome (olive shading)<sup>96,97</sup> **b** Mean annual precipitation in Mongolia (1979–2021, CRU Ts 4.06<sup>93</sup>). **c** Mean summer June–July–August (JJA) temperature for North Mongolia and the globe (area-weighted) between 1950–2021<sup>93,94</sup>, along with CMIP6 projected ensemble median ‘historical’ (1950–2014) and ‘future’ (2015–2100) temperature for both regions (22 models, 54 ensemble members, Supplementary Table 1) relative to their 1961–1990 mean (dashed zero line). Projections are derived using four shared socioeconomic pathways<sup>95,98</sup> (SSP1–2.6; SSP2–4.5; SSP3–7.0; and SSP5–8.5). The ensemble median weights models equally, accounting for variable ensemble member sizes across models. Further, it represents the common warming signal across models and is not expected to replicate the range of interannual variance of the observational data, unlike an individual ensemble member. Future projections are smoothed with a running 5-year mean (Supplementary Fig. 2 shows the model spread). **d** Observed warming in North Mongolia and the globe between 2001–2021 (OBS.) and at the end-of-the-century (2081–2100) using four CMIP6 SSPs (relative to 1961–1990). CMIP6 boxplots represent spread across 54 ensemble members. The red dot and the text at the bottom describe the median warming for observational data and ensemble median warming for CMIP6. Observed JJA warming in North Mongolia is nearly thrice the global average (1.82 °C cf. 0.63 °C, 2001–2021 cf. 1961–1990). The region is projected to warm ~1.7 times the global average through the 21st century, regardless of the SSP used. Same y-axis label in **c** and **d** with different ranges. Each box describes the 25th, 50th (i.e., median) and 75th percentiles of data and whiskers describe the range.

Rising mean temperatures are increasing the frequency and intensity of extreme heat events (i.e. the maximum temperature of the hottest day,  $T_{\text{air-xx}}$ )<sup>26–28</sup>. Changes in regional extreme temperature are expected to be greater than global mean temperature by a factor of 1.5 due to higher climate variability at local scales, differences in specific heat capacities of land and ocean, and feedbacks resulting from decreases in snow and soil moisture<sup>27</sup>. Further, while the intensity of warm extremes is expected to scale linearly with emissions and the degree of global warming, their frequency is expected to scale non-linearly<sup>29</sup>. The highest increase in  $T_{\text{air-xx}}$  magnitude and frequency is projected to occur in mid-latitude regions, including North Mongolia<sup>29</sup>. These changes will have implications for forest ecosystems since all plant metabolic processes, including photosynthetic carbon assimilation, respiration and growth, are negatively impacted by temperature stress<sup>30–33</sup>. Photosystems I and II are two protein complexes that play a fundamental role in carbon assimilation and are located in the thylakoid membranes of plant leaves, where light energy is converted to chemical energy during photosynthesis<sup>34</sup>. The critical temperature of photosystem II (PSII) disruption ( $T_{\text{crit}}$ ) represents a ‘point of no return’ at which leaves start to become irreversibly damaged and photosynthetic electron transport ceases<sup>31,32,35–38</sup>. Sufficient accumulated damage to plants at regional scales can cause forest dieback and act as a trigger for abrupt ecosystem transition<sup>32,35</sup>. Extreme heat in particular has the potential to cause irreversible damage to plant photosynthetic apparatus since leaf temperature can exceed air temperature by +5–20°C depending on radiation load, transpiration, and wind speed<sup>31–33,35,36,39</sup>.

The importance of boreal forests in the global carbon cycle and the increasing probability of exposure to damaging high temperatures call for an urgent assessment of plant physiological thresholds to predict ecological change under a warming climate. However, most boreal thermal tolerance research has focussed on cold and not heat tolerance<sup>29,32</sup> despite boreal plants being particularly vulnerable to warming due to their low thermal safety margins<sup>31</sup>, defined as the difference between  $T_{\text{crit}}$  and the maximal leaf temperature ( $T_{\text{leaf-xx}}$ )<sup>40</sup>. To the best of our knowledge, no characterisation of  $T_{\text{crit}}$  exists for boreal Eurasia or across Asian forest biomes, more generally<sup>32</sup>. Additionally, most large-scale ESMS currently do not include a warm-tolerance threshold in their representation of the temperature dependence of plant carbon assimilation<sup>31</sup>. Exceedance of this warm-tolerance threshold due to climate change can act as a trigger for abrupt ecosystem transition, substantially sooner than the ~50–100-year timescales over which the southern boreal forest transition is currently projected to occur<sup>9,13</sup>.

Here we apply a trait-based vulnerability assessment approach<sup>41,42</sup> to evaluate whether climate change may cause temperature extremes in excess of plant  $T_{\text{crit}}$  at the southern margin of the Eurasian boreal forest. To do so we first comprehensively characterise the physiological responses of five dominant species in boreal North Mongolia by examining their chlorophyll fluorescence parameters, leaf traits, foliar nutrients, and foliar stable isotopes at a study site located in the Targvagai Valley, Bulgan in North Mongolia (red star in Fig. 1a, b). We then evaluate their thermal tolerance traits against CMIP6 ESM-derived temperature projections through the end of the twenty-first century. Species studied here include Siberian larch (*Larix sibirica*), silver birch (*Betula platyphylla*), Siberian elm (*Ulmus pumila*), Eurasian aspen (*Populus tremula*), and willow (*Salix spp.*)<sup>43</sup> (Supplementary Fig. 4). We place special emphasis on *Larix sibirica* since it is a foundation tree species across boreal Eurasia accounting for a third of the biome’s total biomass<sup>44–46</sup>, and 80% of all Mongolian forest biomass where it provides important ecosystem services such as fuel wood and a

productive grazing habitat for livestock<sup>47</sup> (Fig. 1a and Supplementary Fig. 5).

## Results

**Higher photosynthetic capacity but faster activation of photoprotection in *Larix sibirica*.** Light energy reaching plant photosystems follows one of three main pathways<sup>48</sup>. Under favourable conditions, most light energy is used for photosynthetic electron transport (known as photochemistry), while excess energy is dissipated as heat (non-photochemical quenching, NPQ), and a small fraction (0–3%) is remitted as chlorophyll fluorescence<sup>48</sup>. We used Pulse Amplitude Modulated (PAM) chlorophyll fluorescence to estimate the photosynthetic capacity and performance of dark-adapted tree foliage<sup>34,49</sup>. We found that *Larix sibirica* converted a greater proportion of absorbed light energy to photochemistry as indicated by its higher maximum photochemical yield of PSII ( $F_v/F_m$ ) relative to all species (Supplementary Fig. 6a,  $p < 0.05$  except *Salix spp.*, pairwise non-parametric Wilcoxon signed-rank tests<sup>50</sup>).

Rapid Light Curves (RLCs<sup>48</sup>) indicated that *Larix sibirica* consistently achieved higher electron transport rates (ETR) for the same level of actinic irradiance (or photosynthetic photon flux density, PPFD) (Fig. 2a). This pattern of inter-species differences, with the highest values for *Larix sibirica*, was also observed for quantum efficiency ( $\alpha$ ), maximum ETR ( $ETR_{\text{max}}$ ), and minimum saturating irradiance ( $I_k$ ) (Supplementary Fig. 6b–d). There were no consistent differences in ETR for sun and shade leaves (Supplementary Fig. 7). RLCs for photochemistry expressed by the effective quantum yield of PSII ( $\Phi_{\text{PSII}}$ ) and for heat dissipation (NPQ) showed that as irradiance (PAR, photosynthetically active radiation) increased,  $\Phi_{\text{PSII}}$  decreased exponentially while NPQ increased following a saturation curve for all five species<sup>51</sup> (Supplementary Fig. 8).

All species experienced a dynamic reallocation of absorbed light energy from photochemistry to NPQ as irradiance intensity increased, as shown by the negative relationships between  $\Phi_{\text{PSII}}$  and NPQ (Fig. 2b and Supplementary Fig. 9). However, *Larix sibirica* (and *Ulmus pumila*) exhibited stronger and more negative linear relationships between  $\Phi_{\text{PSII}}$  and NPQ indicating higher vulnerability to damage at increasing light levels and a faster activation of photoprotection via NPQ.  $\Phi_{\text{PSII}}$  is a measure of the proportion of light energy absorbed by PSII used in photochemistry, while NPQ is indicative of the amount of absorbed light energy dissipated by changes in the xanthophyll cycle de-epoxidation state (i.e., not used for photochemistry or re-emitted as fluorescence)<sup>48,51</sup>. This dynamic reallocation is associated with increased photoprotection to prevent damage to the photosynthetic apparatus at high light<sup>52</sup>. Nevertheless, *Larix sibirica* maintained a higher ETR and  $\Phi_{\text{PSII}}$  and a lower NPQ relative to all species at all irradiance levels (Supplementary Figs. 8, 9).

*Larix sibirica*’s higher abundance and biomass across the landscape<sup>44,46</sup> may therefore partially be explained by how it outperforms co-located species in carbon assimilation under current climate conditions. An ETR of 4  $\mu\text{mol}/\text{m}^2\text{s}$  (y-axis in Fig. 2a) is theoretically equivalent to a gross photosynthesis rate of 1  $\mu\text{mol}/\text{m}^2\text{s}$  (ref. 51). However, while ETR and  $\text{CO}_2$  assimilation are generally proportional, their relationship can be non-linear for  $\text{C}_3$  plants<sup>51</sup>.  $\text{CO}_2$  assimilation is also a function of the carboxylative activity of the enzyme RuBisCO, which is in-turn influenced by stomatal and mesophyll conductance<sup>34</sup>. Additionally, the oxygenation by RuBisCO instead of carboxylation (photorespiration), cyclic electron transport, and nitrate reduction can be alternative electron sinks to carbon assimilation<sup>34</sup>. Consequently, we analysed the foliar chemistry of all species to further examine *Larix sibirica*’s higher photosynthetic capacity<sup>53</sup>.

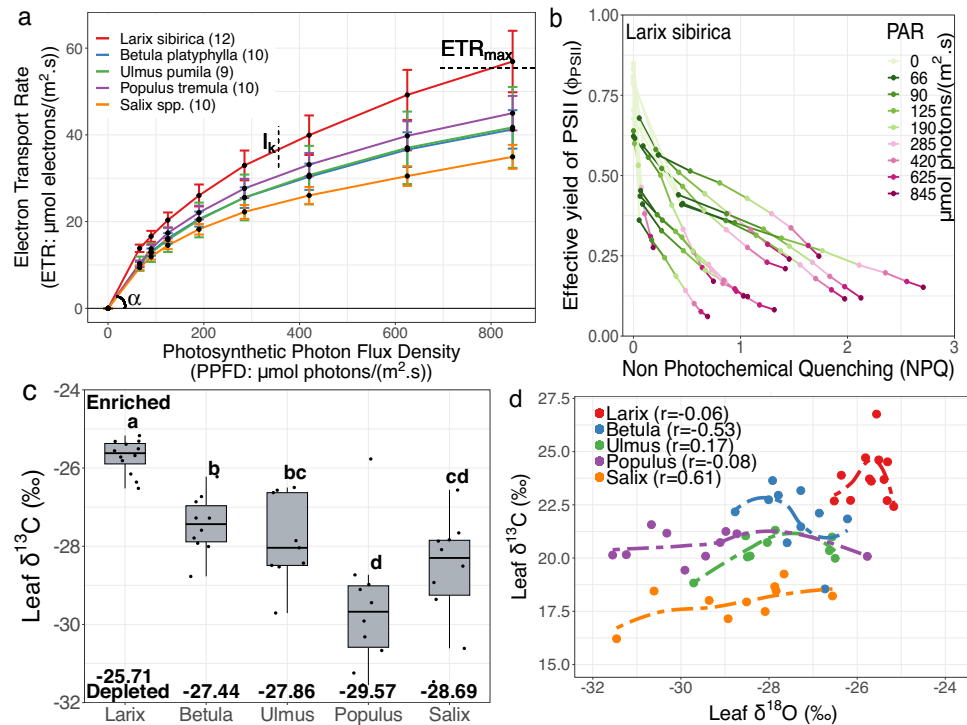


**Fig. 2** Plant photosynthetic performance and foliar isotopes. **a** Electron transport rate (ETR,  $\mu\text{mol-electrons}/(\text{m}^2\cdot\text{s})$ ) against photosynthetic photon flux density (PPFD,  $\mu\text{mol photons}/\text{m}^2\cdot\text{s}$ ). PPFD is the intensity of photosynthetically active radiation (PAR) in the -400–700 nm spectral range that plants can use for photosynthesis<sup>99</sup> (full sunlight is generally between -900–1500  $\mu\text{mol photons}/\text{m}^2\cdot\text{s}$ ). See Supplementary Fig. 6 for quantum efficiency ( $\alpha$ ), maximum ETR ( $ETR_{\text{max}}$ ), and minimum saturating irradiance ( $I_k$ ). Error bars describe  $\pm$  one standard error. The number of sampled leaves is noted in the legend. **b** An inverse relationship between the effective yield of Photosystem II ( $\Phi_{\text{PSII}}$ ) and non-photochemical quenching (NPQ) with increasing PAR in *Larix sibirica*. **c** Foliar  $\delta^{13}\text{C}$  for all species showing that *Larix sibirica* is significantly enriched in  $\delta^{13}\text{C}$  ( $p < 0.05$ , Wilcoxon signed-rank test<sup>50</sup>). Each box describes the 25th, 50th (i.e. median) and 75th percentiles of data and whiskers describe the range. Statistically significant differences are indicated by the lack of a shared letter label between species, while numbers describe the species mean. **d** Scatterplot between foliar  $\delta^{13}\text{C}$  and  $\delta^{18}\text{O}$  for all species, along with a loess fit and Spearman rank correlations.

**Enriched stable carbon isotopic ratios in *Larix sibirica* as a result of high photosynthetic rates.** Foliar stable carbon ( $\delta^{13}\text{C}$ ) and oxygen ( $\delta^{18}\text{O}$ ) isotopic ratios showed a consistent pattern of being most enriched for *Larix sibirica* and most depleted for *Populus tremula* ( $\delta^{13}\text{C}$ ) and *Salix spp.* ( $\delta^{18}\text{O}$ ) (Fig. 2c and Supplementary Fig. 10a). However, foliar  $\delta^{13}\text{C}$  and  $\delta^{18}\text{O}$  were not correlated in *Larix sibirica* (Spearman  $r = -0.06$ , Fig. 2d). Foliar  $\delta^{13}\text{C}$  is influenced by the rate of  $\text{CO}_2$  fixation by the enzyme RuBisCo (photosynthetic rate, A) and stomatal conductance ( $g_s$ ), while foliar  $\delta^{18}\text{O}$  is primarily determined by soil source water and evaporative enrichment in the leaf during transpiration<sup>54,55</sup>. Since stomatal conductance ( $g_s$ ) can be a determinant of both  $\delta^{13}\text{C}$  and  $\delta^{18}\text{O}$ , exploring  $\delta^{18}\text{O}$  in conjunction with  $\delta^{13}\text{C}$  (i.e., the dual-isotope method) can shed some light on whether changes in  $\delta^{13}\text{C}$  are related with the rate of photosynthesis (A) or stomatal conductance ( $g_s$ )<sup>56</sup>. Consequently, as leaf  $\delta^{18}\text{O}$  is not influenced by the rate of photosynthesis (A), we interpret that *Larix sibirica*'s enriched leaf  $\delta^{18}\text{O}$  reflects site-level microclimate differences (Supplementary Fig. 4). Despite being a mesic region overall,  $\delta^{18}\text{O}$  was positively correlated with elevation (Spearman  $r = 0.39$ – $0.42$ ,  $p < 0.01$ ) in correspondence with a gradient of better-drained montane soils that undergo higher evaporative enrichment than river valleys (Supplementary Fig. 10b). The lack of relationship between foliar  $\delta^{13}\text{C}$  and  $\delta^{18}\text{O}$ , together with likely microclimatic causes for the  $\delta^{18}\text{O}$  enrichment, suggests that the enriched  $\delta^{13}\text{C}$  in *Larix sibirica* is likely related to higher rates of carbon assimilation<sup>56,57</sup>.

Photosynthetic capacity can also sometimes be associated with higher nitrogen availability since nitrogen is a building block for

the photosynthetic enzyme RuBisCo<sup>7,58,59</sup>. However, similar foliar  $\delta^{15}\text{N}$  across all species suggests a lack of site or species-level differences in nitrogen availability, source (nitrate/ $\text{NO}_3^-$  cf. ammonium/ $\text{NH}_4^+$ ), or root mycorrhizal associations<sup>57,60,61</sup> (Supplementary Fig. 10c). Supporting this result, *Larix sibirica* leaves had lower foliar nitrogen [N%] and higher carbon [C%] concentrations resulting in higher carbon to nitrogen (C:N) ratios (Supplementary Fig. 11).

Therefore, the high photosynthetic performance in *Larix sibirica* is supported by several lines of evidence such as higher ETRs, quantum efficiency ( $\alpha$ ),  $F_v/F_m$ , and enriched foliar  $\delta^{13}\text{C}$ , but does not seem related to higher nitrogen availability<sup>46</sup>. This higher performance of *Larix sibirica* in relation to other species is likely a species-specific trait that facilitates its current role as a foundation species in the North Mongolian and Eurasian boreal forest.

***Larix sibirica*'s low  $T_{\text{crit}}$  may make it more vulnerable to damage from high temperatures.** *Larix sibirica*  $T_{\text{crit}}$  is 3.5–6.7 °C lower than other North Mongolian species (Fig. 3 and Supplementary Figs. 12, 13). While warm temperatures can decrease plant productivity, warm extremes play a more important role in determining plant mortality, survival, photosynthetic performance, and even plant evolution<sup>30,32</sup>. At  $T_{\text{crit}}$ , minimal chlorophyll-a fluorescence of PSII ( $F_o$ ) begins to rise rapidly, indicating damage to thylakoid membrane where the PSII is located<sup>37,62,63</sup> (Supplementary Fig. 12). An evaluation of  $T_{\text{crit}}$  of *Larix sibirica* in terms of observed and projected  $T_{\text{air-xx}}$  under different SSPs suggests overlap between the lower threshold of the

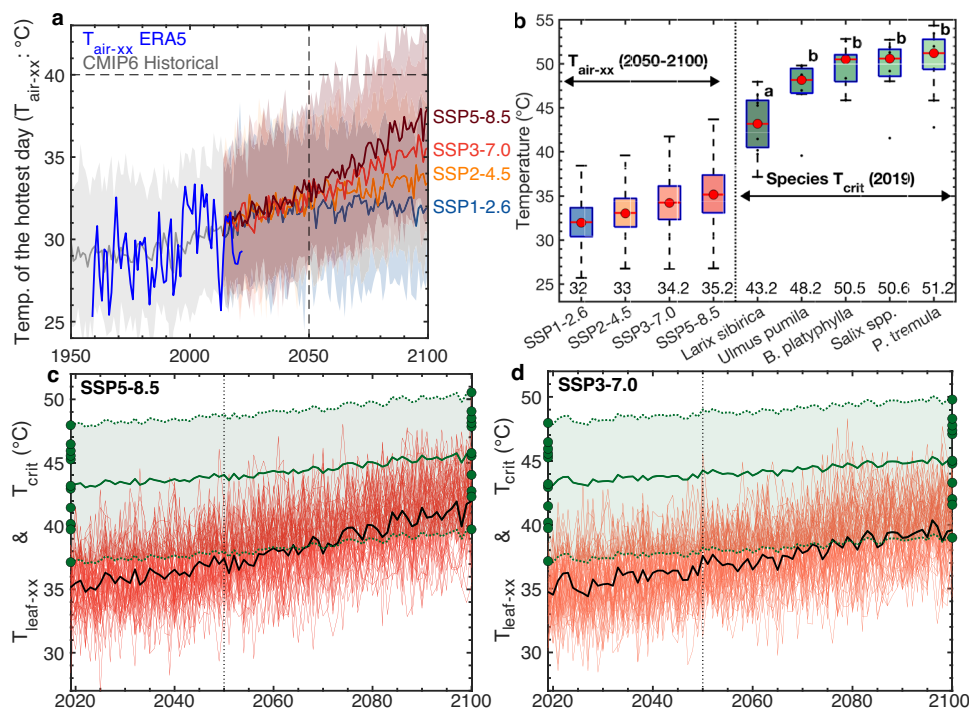


**Fig. 3** Maximum temperature of the hottest day ( $T_{\text{air-xx}}$ ) and hottest leaf temperature ( $T_{\text{leaf-xx}}$ ) in relation to the critical temperature of photosystem II disruption ( $T_{\text{crit}}$ ) for all five study species. **a** ERA5  $T_{\text{air-xx}}$  between 1959–2021 (in blue, averaged across a  $0.2 \times 0.2$ -degree grid box around our study site:  $103.17^\circ\text{E}$ ,  $49.92^\circ\text{N}$ ) along with CMIP6 projected ensemble median ‘historical’ (1950–2014) and ‘future’ (2015–2100)  $T_{\text{air-xx}}$  using 4 four shared socioeconomic pathways (SSPs) (23 models, 56 ensemble members, averaged across a  $1.5 \times 1.5$ -degree grid box around our site). Horizontal and vertical lines represent  $T_{\text{air-xx}}$  of  $40^\circ\text{C}$  and the year 2050, respectively. **b** Range of variability in  $T_{\text{air-xx}}$  between 2050–2100 under different SSPs (red dot: ensemble median) and measurements of the  $T_{\text{crit}}$  of all five study species measured in the field in 2019. Ensemble median  $T_{\text{air-xx}}$  and median  $T_{\text{crit}}$  are described below each boxplot. The lack of a shared common letter label between *Larix sibirica* and all other North Mongolian species indicates that it has a significantly lower  $T_{\text{crit}}$  ( $p < 0.05$  using a non-parametric Wilcoxon signed-rank test<sup>50</sup>). *Larix sibirica*’s measured thermal tolerance range [ $T_{\text{crit-min}}$ ,  $T_{\text{crit-max}}$ ] is  $37.15$ – $47.96^\circ\text{C}$  (mean  $43.25^\circ\text{C}$ , median  $43.18^\circ\text{C}$ ). Each box describes the 25th, 50th (i.e., median) and 75th percentiles of data and whiskers describe the range. **c, d** Projections of future  $T_{\text{leaf-xx}}$  under SSP5-8.5 (**c**) and SSP3-7.0 (**d**) in relation to projections of *Larix sibirica*’s acclimated  $T_{\text{crit}}$  (in green) under the same scenarios (CMIP6 ensemble median in black, individual ensemble members in red).  $T_{\text{leaf-xx}}$  exceeds median  $T_{\text{crit}}$  frequently after ~2050 (dotted vertical black line) under both SSPs suggesting conditions that maximise the potential for sustained damage to *Larix sibirica*’s photosynthetic apparatus.

current thermal tolerance range of *Larix sibirica* and  $T_{\text{air-xx}}$  under SSP3-7.0 and SSP5-8.5 in the second half of this century (2050–2100) (Fig. 3a, b). These results indicate that *Larix sibirica* is more vulnerable to damage to its photosynthetic apparatus than other co-located species in North Mongolia and would be more frequently exposed to damaging summer temperatures exceeding its  $T_{\text{crit}}$  as summer temperatures continue to warm through this century<sup>32,37,53,63,64</sup> (Fig. 1c and Supplementary Fig. 2a).

The  $T_{\text{crit}}$  of a species may, however, acclimate with warming<sup>31,32,65</sup>. Acclimation in some species can occur seasonally, with lower  $T_{\text{crit}}$  during cool winter months (in evergreen species) and higher  $T_{\text{crit}}$  during summer months, or under exposure to warmer growing conditions<sup>63,66</sup>. In a global survey of temperature responses,  $T_{\text{crit}}$  increased on average by  $0.38^\circ\text{C}$  per  $^\circ\text{C}$  increase in the mean maximum temperature of the warmest month<sup>31</sup>. This global increase in  $T_{\text{crit}}$  with temperature is greater than the observed regional and seasonal acclimatisation of  $T_{\text{crit}}$ <sup>38,63,67</sup>. We, therefore, applied a  $0.38^\circ\text{C}$  increase in  $T_{\text{crit}}$  per  $^\circ\text{C}$  increase in the ensemble median  $T_{\text{air-xx}}$  as an optimistic upper-range estimate of thermal acclimation of  $T_{\text{crit}}$  for *Larix sibirica* (Supplementary Fig. 13b). Nevertheless, we note that the mechanisms of thermal acclimation are poorly understood<sup>63,68</sup>. It is uncertain whether  $T_{\text{crit}}$  acclimates in all species, particularly in deciduous species such as those studied here, and whether there are limits to the degree of acclimation<sup>63,69</sup>. Additionally, the

rate of increase in temperature due to climate change is projected to be greater than the rate of  $T_{\text{crit}}$  acclimation (see the following section). Therefore, while thermal acclimation may potentially moderate some of the impacts of extreme  $T_{\text{air-xx}}$ <sup>68</sup> it is likely that *Larix sibirica* may be more vulnerable to rising temperature if its  $T_{\text{crit}}$  acclimates at a slower pace or negligible pace than assumed here.

**Leaf temperature exceeds *Larix sibirica*’s  $T_{\text{crit}}$  under high emission scenarios by 2050.** Leaf temperature ( $T_{\text{leaf}}$ ) is a more relevant metric to evaluate plant thermal tolerance since  $T_{\text{leaf}}$  can exceed air temperature by  $+5$ – $20^\circ\text{C}$ <sup>31,32,38,40,70</sup>. On diurnal timescales, photosynthesis and stomatal conductance generally decrease during the early afternoon due to high temperature and a high leaf-to-air vapour pressure gradient<sup>71–73</sup>. At longer daily to seasonal timescales, stomatal closure can occur during drought conditions<sup>30</sup>. Partial to full stomatal closure during the ‘mid-day depression’ of photosynthesis and during drought reduce plant transpiration and associated latent heat flux cooling and enhances leaf temperature above air temperature<sup>30,72,74</sup>.

Higher  $T_{\text{leaf}}$  can be expected regionally in coming decades as a result of increased stomatal closure from enhanced VPD,  $T_{\text{air}}$ , atmospheric  $\text{CO}_2$  and the lack of projected increases in precipitation<sup>24,74</sup> (Figs. 3, 1c and Supplementary Figs. 1–3). To overcome the lack of field measurements of  $T_{\text{leaf}}$  we used ERA5 surface skin temperature ( $T_{\text{skin}}$ ) as a proxy for  $T_{\text{leaf}}$  (by

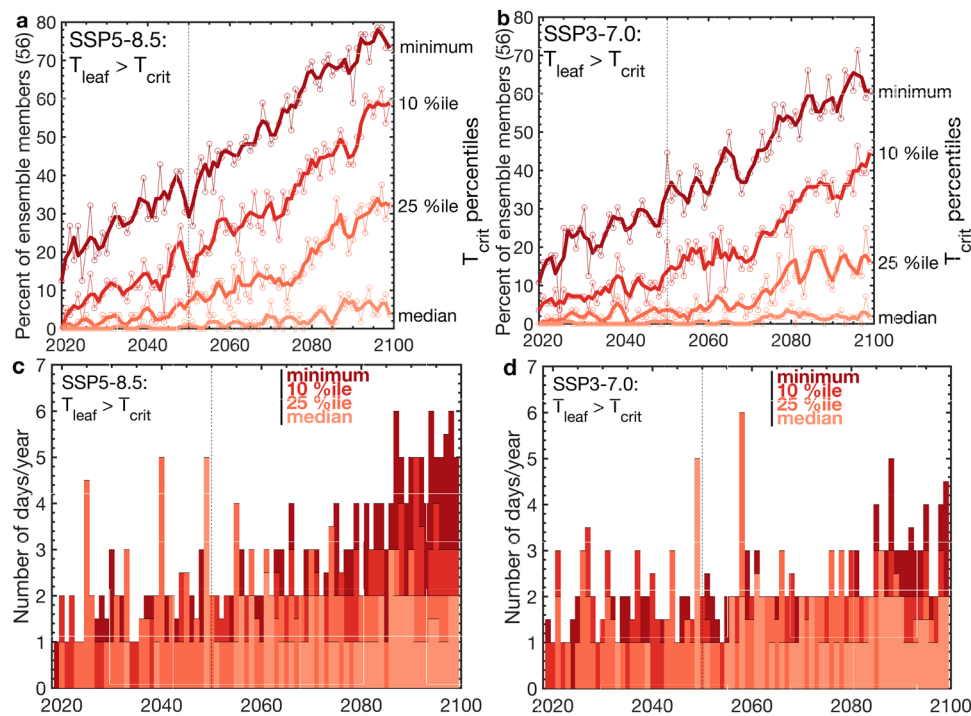


**Fig. 4** Projections of rising intensity and frequency of leaf temperature ( $T_{\text{leaf}}$ ) in excess of the *Larix sibirica*'s  $T_{\text{crit}}$ . The percentage of ensemble members and the median number of days per year when  $T_{\text{leaf}}$  exceeds different  $T_{\text{crit}}$  thresholds under SSP5-8.5 (**a**, **c**) and SSP3-7.0 (**b**, **d**). Thresholds shown are the minimum, 10th percentile, 25th percentile and median  $T_{\text{crit}}$  values, assuming that  $T_{\text{crit}}$  also acclimates to warming temperature. Results are computed across 56 ensemble members from 23 CMIP6 earth system models (ESMs). Despite the exceedance of  $T_{\text{crit}}$  by  $T_{\text{leaf}}$  generally being a low-probability extreme event due to natural year-to-year climate variability, increases are projected both in the likelihood (percent of ensemble members) and magnitude (number of days/year) of  $T_{\text{crit}}$  exceedances each year starting ~2050 across multiple models and model ensemble members. The solid line in **a** and **b** is a 3-yr running average.

setting  $T_{\text{leaf}}$  equal to  $T_{\text{skin}}$ ). Doing so allows us to estimate the leaf temperature ( $T_{\text{leaf}}$ ) in relation to  $T_{\text{air}}$ .  $T_{\text{skin}}$  is the approximate theoretical temperature required to satisfy the surface energy balance<sup>75</sup>, and represents how hot an object would feel to touch since sun-exposed objects can become considerably warmer than surrounding 2 m air temperature<sup>76</sup>. The climatology of our site shows that  $T_{\text{air}}$ ,  $T_{\text{skin}}$ , and precipitation peak during the summer JJA months (Supplementary Fig. 14). Further,  $T_{\text{skin-xx}}$  is generally 1–6 °C warmer than  $T_{\text{air-xx}}$  (Supplementary Fig. 15) with a ~4 °C difference between median  $T_{\text{skin-xx}}$  and  $T_{\text{air-xx}}$ . We apply this 4 °C offset to  $T_{\text{air-xx}}$  projections as an estimate of  $T_{\text{leaf-xx}}$ . This offset is conservative since it is calculated over a coarse spatiotemporal field (a  $0.2^\circ \times 0.2^\circ$  spatial resolution hourly reanalysis data), assumes an infinitesimally thin surface layer without thermal memory, and is considerably lower than field estimates<sup>31,32,36</sup>. Despite this, we find marked increases in the likelihood that  $T_{\text{leaf-xx}}$  exceeds *Larix sibirica*'s warming-acclimated  $T_{\text{crit}}$  by 2050 under the higher emission scenarios SSP5-8.5 and SSP3-7.0, but not under lower emission scenarios SSP2-4.5 and SSP1-2.6 (Fig. 3c, d and Supplementary Figs. 16, 17).

Under the high-emission SSP5-8.5 and SSP3-7.0 scenarios, starting around 2050, annual  $T_{\text{leaf}}$  exceeds the 10th to 25th percentile of *Larix sibirica*  $T_{\text{crit}}$  at least one day per year in 5–20% of CMIP6 simulations (Fig. 4a, b and Supplementary Fig. 18) and *Larix sibirica*'s median  $T_{\text{crit}}$  in 2–10% of the 56 CMIP6 ensemble members (Supplementary Fig. 19). Additionally, the 25th percentile of *Larix sibirica*'s  $T_{\text{crit}}$  is exceeded a median of 2 to 3 days per year in SSP5-8.5 and up to 2 days per year under SSP3-7.0 around 2050 (Fig. 4c, d and Supplementary Fig. 19). Similar results are found for SSP5-8.5 and SSP3-7.0 using only one ensemble member per model and avoiding overweighting models

with more than one ensemble member at the expense of lower sample size of model runs (Supplementary Fig. 20).

In addition to climate change-driven warming, annual  $T_{\text{leaf}}$  and  $T_{\text{air}}$  are also controlled by natural year-to-year climate variability. Therefore, although the exceedance  $T_{\text{crit}}$  by  $T_{\text{leaf}}$  in any given year should theoretically be a low-probability event, we show that exceedances of *Larix sibirica*'s 25th percentile of  $T_{\text{crit}}$  occur across 22 of 23 ESMs used (Supplementary Fig. 21). This suggests that there is potential for damage to *Larix sibirica*'s photosynthetic apparatus in the next three decades by ~2050 under SSP5-8.5 and SSP3-7.0 and that these results are not biased by choice of CMIP6 models used in the presented analysis. However, we note that damage is unlikely under lower emission scenarios (SSP2-4.5 and SSP1-2.6; Supplementary Figs. 16, 17), and projected damage to *Larix sibirica*'s photosynthetic apparatus generally remains less than 60% under the two high emission scenarios SSP5-8.5 and SSP3-7.0 (Supplementary Fig. 18).

## Discussion

Boreal ecosystems contain about one-third of the total terrestrial carbon stock and account for approximately one-third of the annual terrestrial carbon sink<sup>2,77</sup>. A decreased boreal forest carbon sink and release of current carbon stocks following large scale forest mortality can potentially contribute to a 'positive climate feedback' and exacerbate ongoing warming<sup>78</sup>, although we note that net radiative forcing will also depend on surface albedo change<sup>9</sup>. Further, boreal regions in the northern hemisphere have warmed considerably faster than the global average<sup>29,79</sup>. JJA temperatures in North Mongolia have warmed approximately three times the global average (1.81 °C cf. 0.63 °C)

over the past few decades (2001–2021 relative to 1961–1990) and are expected to continue to warm more rapidly than the globe under a range of low to high emission scenarios (Fig. 1 and Supplementary Fig. 2).

Extreme heat can cause permanent damage to a plant's photosynthetic apparatus and can reduce carbon assimilation by forests<sup>31,32</sup>. Damage to the photosynthetic apparatus can occur at the time scale of seconds to minutes following heat exposure<sup>35</sup>. Additionally, forests are highly sensitive to hot temperature extremes at the warm margins of a biome or species distribution range<sup>41,42</sup>. By applying a trait-based vulnerability assessment approach<sup>41,42</sup>, we found that *Larix sibirica* had a significantly lower  $T_{crit}$  among other co-located species in the southern margin of the Eurasian boreal forest (Fig. 3b). Further, we project increases in the frequency, magnitude, and duration of exceedances of *Larix sibirica*'s  $T_{crit}$  using a suite of 23 CMIP6 ESMs (56 ensemble members) if greenhouse gas emissions are not reduced rapidly within the next two decades.  $T_{crit}$  exceedances are projected to occur almost annually starting ~2050 under higher emission scenarios (SSP5-8.5 and SSP3-7.0), but not under lower emission scenarios (SSP2-4.5 and SSP1-2.6) (Figs. 3, 4). The rise in frequency and duration of heat extremes under high emission scenarios, measured by the number of days per year that  $T_{leaf}$  exceeds  $T_{crit}$ , is likely to be particularly deleterious to plant health. While trees can recover from a single stress event if they occur infrequently, frequent and repeated exposure to stress may lead to accumulated damage and exhaustion of carbohydrate reserves<sup>39,80</sup>. This can weaken plant resilience enough that even moderate stress might cause whole plant mortality<sup>39,80</sup>. Additionally, we project increasing aridity in the region due to a higher VPD caused by increasing temperature and a lack of a compensating increase in precipitation<sup>24</sup>. While we assume a conservative 4 °C offset between  $T_{air-xx}$  and  $T_{leaf-xx}$  we note that plants may be more vulnerable to heat damage in the future as stomatal closure due to enhanced drought stress and elevated atmospheric CO<sub>2</sub> can elevate leaf temperature<sup>25,81</sup>.

The  $T_{crit}$  of a species has been hypothesised to be related to the temperature of the environment it evolved or is currently distributed in (evolutionary influence on  $T_{crit}$ ), the temperature regime of the local site (phenotypic influence on  $T_{crit}$ )<sup>32,63,65</sup>, and soil moisture availability<sup>81</sup>. The differences in  $T_{crit}$  observed here among the five species cannot however be explained by elevation differences alone (Supplementary Fig. 13) or micro-site differences in soil moisture. Among the four species for which distribution maps are available, *Larix sibirica* is the only species that is located at the southernmost margin of its distribution range at our study site<sup>44,46</sup> (Fig. 1a and Supplementary Fig. 4b). The remaining three species (*Betula platyphylla*, *Ulmus pumila*, and *Populus tremula*) are also distributed further southeast of our study site in warmer and drier localities (Supplementary Fig. 22)<sup>82,83</sup>. Thermal tolerance has also been shown to be higher for species in more humid sites since wetter soils may allow leaves to keep their stomata open for longer and benefit more from evaporative cooling at the leaf surface<sup>81</sup>. In this regard, while *Larix sibirica*'s lower  $T_{crit}$  relative to other species is unexpected at the site-scale based on its preference for drier micro-habitat conditions in better-drained soils away from the river valley (Supplementary Fig. 4a), it could be related to its more northerly distribution in mesic boreal Eurasia.

The lower  $T_{crit}$  of *Larix sibirica* and *Ulmus pumila* relative to other species (Fig. 3b) is also supported by the stronger negative linear relationship between  $\Phi_{PSII}$  and NPQ observed for these two species (Supplementary Fig. 9). The relative rate of increase in NPQ compared to  $\Phi_{PSII}$  at moderate to high PAR values is greater for *Larix sibirica* and *Ulmus pumila* than other species which suggests the need for enhanced photoprotective mechanisms at lower light levels. This suggests that they are more 'vulnerable' to

damage at increasing light. Other species generally show a non-linear response between  $\Phi_{PSII}$  and NPQ and can maintain relatively low NPQ under moderate light levels. Nonetheless, *Larix sibirica* likely outperforms all species in photosynthetic performance as suggested by chlorophyll fluorescence and foliar stable carbon isotopic data (Fig. 2). This higher photosynthetic performance is not related to differences in nitrogen availability (Supplementary Figs. 10, 11) and is also likely a species-specific trait<sup>46</sup> that enables *Larix sibirica* to be highly successful in the Eurasian boreal forest under current climate conditions.

Since *Larix sibirica* is a foundation species across 30% of the Eurasian boreal forest and is the most common tree in Mongolia<sup>47,84</sup>, an increase in the frequency and intensity of extreme heat events in excess of its  $T_{crit}$  may represent a thermal tolerance tipping point at the southern margin of the Eurasian boreal forest. Without rapid emission reductions within the next two to three decades prior to ~2050, our results suggest that the viability of *Larix sibirica* in the boreal forests of Mongolia will likely be threatened by repeated incidences of damage to its photosynthetic apparatus. Combined with the increased likelihood of additional disturbance agents such as drought, fire, insects, and pathogens<sup>85</sup>, such damage has the potential to result in large-scale mortality of *Larix sibirica*-dominated forests, as has already been observed in some locations (Supplementary Fig. 23), and a possible conversion of the ecosystem into a grassland-steppe biome<sup>86</sup>. These changes will likely have significant implications for the region's forestry and herding sectors. However, we do note that our projections of future  $T_{leaf-xx}$  generally do not exceed the 60th percentile of *Larix sibirica*'s  $T_{crit}$  and never exceed its maximum  $T_{crit}$  under either high emission scenario SSP5-8.5 and SSP3-7.0. This suggests a scenario where *Larix sibirica* individuals growing in favourable microclimate conditions (e.g., on cooler north-facing high-elevation slopes) might be able to escape substantial damage from the increasing incidences of extreme heat events.

Additionally, we also acknowledge a few limitations inherent in the sampling design of our study that may contribute to additional uncertainty. We only targeted mature dominant trees at one site in Northern Mongolia in one year, during the warmest part of the year (~5 species × 5 individuals × 2 samples/individual, in July–August 2019). Our results, therefore, may not adequately characterise the within-species variation of the measured traits ( $T_{crit}$ , RLCs, foliar chemistry) both at the site and across boreal Eurasia, their dependence on stand age and density, their variability across years and during the course of the year (note that all species are deciduous). In this regard, we were primarily limited by the time-intensive nature of running over 50 RLCs and temperature-fluorescence curves that took more than one hour per sample in a very remote location without access to grid electricity. We conducted our sampling during the summer months of July and August since plant physiological parameters, including photosynthetic performance and warm thermal tolerance, exhibit seasonal patterns in temperate and boreal climates and generally reach their peak values during the summer months<sup>69</sup>. Tracking of plant physiological parameters through the active season will therefore aid in more fully evaluating plant stress tolerance, for example, to spring season heatwaves when plant  $T_{crit}$  are at their lowest relative values to temperature, but are beyond the scope of this work. Additional plant ecophysiological analyses are therefore needed to more fully characterise the range of spatial and temporal plant thermal tolerance and physiological variability across boreal Eurasia to comprehensively assess the biome's vulnerability to climate change. Further, in our study, we focus on the frequencies of extreme heat events ( $T_{leaf}$  in excess of  $T_{crit}$ ) and not on the absolute magnitude of future  $T_{leaf}$  itself. Downscaled and bias-corrected CMIP6 ESM output (e.g. ref. <sup>87</sup>) can be used to better characterise changes in the magnitude of future extreme heat events (in °C) in

the region, particularly in relation to the exceedance of plant  $T_{crit}$ , though we note that they should not adjust the frequency of extreme heat events.

## Conclusions

Analysis of tipping points in the southern boreal biome margin using ESMs have suggested that large-scale forest dieback will likely occur under high emission scenarios (SSP3-7.0 and SSP5-8.5) by the end of this century over timescales of ~50–100 years<sup>9,13</sup>. However, the relationships between forest mortality and disturbance agents such as fire, drought and insects are poorly characterised in ESMs<sup>88</sup>. Additionally, most ESMs currently represent the temperature dependence of plant carbon assimilation using Arrhenius-type functions that assume a thermal optimum for photosynthesis and a fully reversible decline in photosynthesis at high leaf temperature<sup>35,89</sup>, while in-situ studies show that even a few minutes of exposure of leaves to temperatures in excess of  $T_{crit}$  can cause long-term damage to plant photosynthetic apparatus and result in tissue necrosis<sup>35</sup>. Consequently, it is possible that we may currently be underestimating the timing and rate of southern boreal biome ecosystem change<sup>88</sup>. Here we identify potential mechanisms for an abrupt thermal tipping point in southern boreal Eurasia due to projected increases in the frequency and intensity of extreme heat events ( $T_{air-xx}$ ) under continued climate change that may cause  $T_{leaf}$  to exceed  $T_{crit}$ . Such exceedances, particularly if they occur in close succession<sup>80</sup>, may act as a trigger for regional-scale forest mortality on timescales of days to years. Though we note that eventual tree death will likely be caused by a combination of multiple stress factors such as hydraulic failure, depletion of carbon reserves, drought, insects, and pathogens, in addition to direct heat damage. We find that this tipping point may be exceeded as soon as 2050 under high-emission trajectories (SSP3-7.0 and SSP5-8.5)<sup>90</sup>, significantly sooner than prior ESM estimates that predict ecosystem transitions to occur at the end of this century over decadal to centennial timescales. Incorporating plant  $T_{crit}$  in the next generation of ‘trait-based’ vegetation models and ESMs will therefore be important to accurately simulate the future terrestrial carbon cycle both globally and in the Eurasian boreal forest.

## Methods

**Study site and foliar sampling.** Our study site is located at 103.17°E, 49.92°N in the Tarvagatai River valley in the Bulgan aimag (province) of north-central Mongolia and east of the Teshig soum. The Tarvagatai Valley is located in the forest-steppe region of the Baikal Rift Zone and has a basal elevation of ~900 m above sea level<sup>91</sup>. The river Tarvagatai originates in the Khantai mountains and flows through this valley, eventually joining the Eg river and forming one of the largest rivers in Northern Mongolia<sup>43</sup>. The regional climate is strongly seasonal, with long and cold winters and short but warm summers (Supplementary Fig. 14)<sup>43</sup>. In total, 53 leaves were collected from a total of 25 trees (5 trees × 5 species). On average, we collected two leaves per tree (25 trees × 2 leaves/tree), with a sun leaf collected on the south-facing aspect and a shade leaf collected on a north-facing aspect. We collected leaves at multiple elevations within ~5–7 km of the study site on dominant tree individuals.

**Rapid light curves (RLC), foliar chemistry and critical temperature of PSII disruption ( $T_{crit}$ ).** We made RLC measurements using the Junior PAM portable chlorophyll fluorometer (Heinz Walz GmbH). Each RLC consists of the fluorescence responses to nine different increasing actinic irradiances (i.e. light energy that can trigger plant photochemistry) ranging from 0 through 845  $\mu\text{mol photons/m}^2\text{s}$ . The Junior PAM fluorometer is fitted with a 1.5 mm diameter fibre optic and a blue diode (485 ± 40 nm) with an attachable magnetic clamp on one end that holds down the leaf specimen to ~1 mm from the end of the optic fibre<sup>51</sup>. We measured PAM parameters such as the Electron Transport Rate (ETR), the quantum efficiency of photosynthesis ( $\alpha$ ), non-photochemical quenching (NPQ), etc., using the WINCONTROL-3 software. The apparent rate of photosynthetic electron transport of PSII (ETR) was obtained as:

$$\text{ETR} = \Phi_{\text{PSII}} * \text{PPFD} * 0.5 * 0.84$$

where, PPFD represents the photosynthetic photon flux density (in  $\mu\text{mol photons/}$

$\text{m}^2\text{s}$ ) of the applied actinic irradiance. The effective quantum yield of photosystem II ( $\Phi_{\text{PSII}}$ ) is calculated as  $(F_m' - F)/F_m'$ , where  $F_m'$  is the maximal fluorescence after each incremental light pulse and  $F$  is the fluorescence during light treatment. The scaling factor of 0.5 assumes equal excitation of both PSII and PSI, while the absorbance factor of 0.84 is an estimate of the fraction of incident light that is actually absorbed by PSII<sup>48,92</sup>. Prior to performing the RLCs, all leaves were wrapped in moist paper towels and were placed in the dark for a minimum of 2 h. This dark adaptation minimises the impact of reversible photoinhibition by permitting the dissipation of the electrochemical gradient across the thylakoid membrane<sup>48</sup>. However, to further drain electrons from the acceptor side of PSII and fully oxidise it we applied a 5.5 s far-red-light ( $6 \mu\text{mol m}^{-2} \text{s}^{-1}$ ) treatment prior to all measurements<sup>48</sup>. RLCs were conducted with leaf temperatures around 20 °C. Following an RLC, each leaf was allowed to rest in the dark under the magnetic leaf clip for ~5 min until minimal chlorophyll-a fluorescence levels stabilised, after which another 5.5 s far red-light treatment were applied on the leaves<sup>53</sup>. Finally, each leaf was heated from 20 °C to 60 °C at a rate of ~1 °C/min and minimal chlorophyll-a fluorescence was measured continuously using the Junior PAM device to produce fluorescence-temperature (FT) curves (Supplementary Fig. 12).  $T_{crit}$  was determined by fitting a piecewise best-fit linear regression to each FT curve<sup>31</sup>.

We then dried each leaf for a minimum of 48 h at 60 °C in a drying oven and ground them in separate vials using a ball mill grinder. Following this, we determined leaf percent carbon (%C), percent nitrogen (%N), percent oxygen (%O) using an elemental analyser (ECS 4010, Costech Analytical Technologies, Inc., Valencia, California, USA), and leaf  $\delta^{13}\text{C}$ ,  $\delta^{18}\text{O}$  and  $\delta^{18}\text{O}$  using an isotope ratio mass spectrometer (Delta PlusXP, Thermo Finnigan, Bremen, Germany).

**Climate and Earth system models.** We derived climate data from three datasets, (i) CRU Ts 4.06 monthly data<sup>93</sup>, (ii) HadCRU5<sup>94</sup> and (iii) ERA5<sup>75</sup>. We downloaded the earth system model (ESM) output from the Coupled Model Inter-comparison Project (CMIP6) archive at PANGEO (<https://pangeo-data.github.io>). CMIP6 includes a suite of model experiments organised and contributed from multiple modelling centres in support of the Sixth Assessment Report (AR6) of the Intergovernmental Panel on Climate Change (IPCC)<sup>23,95</sup>. Our analysis is restricted to models that had continuous ensemble members spanning the ‘historical’ (1950–2014 C.E.) and ‘future’ (2015–2100 C.E.) time periods to allow for a comparison between model simulated ‘historical’ and ‘end-of-the-century’ climate on a model-by-model basis. Further, we only used ESMs that had both daily and monthly model outputs available on PANGEO. This resulted in a subset of 23 models and 56 ensemble members (Supplementary Table 1). However, for analysis of monthly temperature data, only 22 models and 54 ensemble members are considered as the historical period temperature data was not available for MPI-ESM1-2-HR (footnote in Supplementary Table 1).

To calculate projections of summer JJA temperature and precipitation (Fig. 1 and Supplementary Figs. 2, 3) we first downloaded monthly 2 m near-surface air temperature (variable tas) and monthly precipitation flux (variable pr) for the globe and for North Mongolia (46–52°N, 95–114°E) from the CMIP6 archive. Next, we converted the monthly precipitation flux ( $\text{kg}/(\text{m}^2\text{s})$ ) into monthly precipitation (in mm). We then calculated all climate series (ERA5 temperature, CRU Ts 4.06 precipitation, all CMIP6 ensemble members) for the globe and for North Mongolia relative to their 1961–1990 mean. Following this, we computed  $T_{air-xx}$  as the maximum temperature of the hottest day of each year using ERA5 and CMIP6 data. To achieve this for ERA5, we first calculated the daily maximum  $T_{air}$  using hourly ERA5 data, while for CMIP6 data, we directly downloaded daily maximum temperature data for each model ensemble member (variable tasmax). CMIP6 tasmax data were averaged across a  $1.5 \times 1.5$ -degree latitude-longitude grid box around our site for projections of  $T_{air-xx}$ . To develop projections of  $T_{air-xx}$  we first adjusted the mean  $T_{air-xx}$  of each ensemble member between 1979 and 2014 to match the mean ERA5  $T_{air-xx}$  for the same period. We applied this ‘mean correction’ since 45 of the 56 CMIP6 ensemble members exhibited a ‘warm bias’ relative to ERA5 data (Supplementary Fig. 24). On average, CMIP6 projections of  $T_{air-xx}$  would be 1.67 °C warmer without this mean value adjustment.

## Data availability

Ecophysiology data is available within Supplementary Data 1. All data and associated code are publicly available at Dryad and Zenodo at <https://doi.org/10.25338/B8TD2T> and may also be requested from the lead author Rao.

## Code availability

All code is publicly available on Dryad <https://doi.org/10.25338/B8TD2T>, via Zenodo <https://doi.org/10.5281/zenodo.7770697>. They may also be requested from the lead author Rao.

Received: 29 September 2022; Accepted: 26 June 2023;

Published online: 10 July 2023



## References

- Malhi, Y., Baldocchi, D. D. & Jarvis, P. G. The carbon balance of tropical, temperate and boreal forests. *Plant Cell Environ.* **22**, 715–740 (1999).
- Pan, Y. et al. A large and persistent carbon sink in the World's forests. *Science* **333**, 988–993 (2011).
- Bradshaw, C. J. A., Warkentin, I. G. & Sodhi, N. S. Urgent preservation of boreal carbon stocks and biodiversity. *Trends Ecol. Evol.* **24**, 541–548 (2009).
- Bradshaw, C. J. A. & Warkentin, I. G. Global estimates of boreal forest carbon stocks and flux. *Global Planet. Change* **128**, 24–30 (2015).
- Goulden, M. L. et al. Sensitivity of boreal forest carbon balance to soil thaw. *Science* **279**, 214–217 (1998).
- Scheffer, M., Hirota, M., Holmgren, M., Van Nes, E. H. & Chapin, F. S. Thresholds for boreal biome transitions. *Proc. Natl Acad. Sci. USA* **109**, 21384–21389 (2012).
- Wright, I. J. et al. The worldwide leaf economics spectrum. *Nature* **428**, 821–827 (2004).
- Kakinuma, K., Yanagawa, A., Sasaki, T., Rao, M. P. & Kanae, S. Socio-ecological Interactions in a changing climate: a review of the Mongolian pastoral system. *Sustainability* **11**, 5883 (2019).
- Armstrong McKay, D. I. et al. Exceeding 1.5°C global warming could trigger multiple climate tipping points. *Science* **377**, eabn7950 (2022).
- Gauthier, S., Bernier, P., Kuuluvainen, T., Shvidenko, A. Z. & Schepaschenko, D. G. Boreal forest health and global change. *Science* **349**, 819–822 (2015).
- Berner, L. T. & Goetz, S. J. Satellite observations document trends consistent with a boreal forest biome shift. *Global Change Biol.* <https://doi.org/10.1111/gcb.16121> (2022).
- Rotbarth, R. et al. Northern expansion is not compensating for southern declines in North American boreal forests. *Nat. Commun.* **14**, 3373 (2023).
- Lenton, T. M. et al. Tipping elements in the Earth's climate system. *Proc. Natl Acad. Sci. USA* **105**, 1786–1793 (2008).
- Davi, N. K. et al. A long-term context (931–2005 C.E.) for rapid warming over Central Asia. *Quat. Sci. Rev.* **121**, 89–97 (2015).
- Hessl, A. E. et al. Past and future drought in Mongolia. *Sci. Adv.* **4**, e1701832 (2018).
- Davi, N. K. et al. Accelerated recent warming and temperature variability over the past eight centuries in the Central Asian Altai from blue intensity in tree rings. *Geophys. Res. Lett.* **48**, e2021GL092933 (2021).
- Pederson, N., Hessl, A. E., Baatarbileg, N., Anchukaitis, K. J. & Di Cosmo, N. Pluvials, droughts, the Mongol Empire, and modern Mongolia. *Proc. Natl Acad. Sci. USA* **111**, 4375–4379 (2014).
- Previdi, M., Smith, K. L. & Polvani, L. M. Arctic amplification of climate change: a review of underlying mechanisms. *Environ. Res. Lett.* **16**, 093003 (2021).
- Dulamsuren, C. et al. Increased summer temperatures reduce the growth and regeneration of *Larix sibirica* in southern boreal forests of Eastern Kazakhstan. *Ecosystems* **16**, 1536–1549 (2013).
- Rao, M. P. et al. Dzuds, droughts, and livestock mortality in Mongolia. *Environ. Res. Lett.* **10**, 074012 (2015).
- Haraguchi, M. et al. Estimating return intervals for extreme climate conditions related to winter disasters and livestock mortality in Mongolia. *Nat. Hazards Earth Syst. Sci. Discuss.* **2021**, 1–26 (2021).
- John, R. et al. Vegetation response to extreme climate events on the Mongolian Plateau from 2000 to 2010. *Environ. Res. Lett.* **8**, 035033 (2013).
- Eyring, V. et al. Overview of the coupled model intercomparison project phase 6 (CMIP6) experimental design and organization. *Geosci. Model Dev.* **9**, 1937–1958 (2016).
- Cook, B. I., Smerdon, J. E., Seager, R. & Coats, S. Global warming and 21st century drying. *Clim. Dyn.* **43**, 2607–2627 (2014).
- Lesk, C. et al. Compound heat and moisture extreme impacts on global crop yields under climate change. *Nature Rev. Earth Environ.* **3**, 872–889 (2022).
- Dosio, A., Mentaschi, L., Fischer, E. M. & Wyser, K. Extreme heat waves under 1.5 °C and 2 °C global warming. *Environ. Res. Lett.* **13**, 054006 (2018).
- Seneviratne, S. I., Donat, M. G., Pitman, A. J., Knutti, R. & Wilby, R. L. Allowable CO<sub>2</sub> emissions based on regional and impact-related climate targets. *Nature* **529**, 477–483 (2016).
- Diffenbaugh Noah, S. et al. Quantifying the influence of global warming on unprecedented extreme climate events. *Proc. Natl Acad. Sci. USA* **114**, 4881–4886 (2017).
- Seneviratne, S. I. et al. in *The Physical Science Basis. Contribution of Working Group I to the Sixth Assessment Report of the Intergovernmental Panel on Climate Change* (eds V. Masson-Delmotte, V. et al.) Ch. 11 (Intergovernmental Panel on Climate Change (IPCC), 2021).
- Reichstein, M. et al. Climate extremes and the carbon cycle. *Nature* **500**, 287–295 (2013).
- O'sullivan, O. S. et al. Thermal limits of leaf metabolism across biomes. *Global Change Biol.* **23**, 209–223 (2017).
- Geange, S. R. et al. The thermal tolerance of photosynthetic tissues: a global systematic review and agenda for future research. *New Phytol.* **229**, 2497–2513 (2021).
- Doughty, C. E. & Goulden, M. L. Are tropical forests near a high temperature threshold? *J. Geophys. Res. Biogeosci.* <https://doi.org/10.1029/2007JG000632> (2008).
- Kalaji, H. M. et al. Frequently asked questions about chlorophyll fluorescence, the sequel. *Photosynth. Res.* **132**, 13–66 (2017).
- Hüve, K., Bichele, I., Rasulov, B. & Ninemets, Ü. When it is too hot for photosynthesis: heat-induced instability of photosynthesis in relation to respiratory burst, cell permeability changes and H<sub>2</sub>O<sub>2</sub> formation. *Plant Cell Environ.* **34**, 113–126 (2011).
- Vogel, S. Leaves in the lowest and highest winds: temperature, force and shape. *New Phytol.* **183**, 13–26 (2009).
- Schreiber, U. & Berry, J. A. Heat-induced changes of chlorophyll fluorescence in intact leaves correlated with damage of the photosynthetic apparatus. *Planta* **136**, 233–238 (1977).
- Feeley, K. et al. The thermal tolerances, distributions, and performances of tropical Montane tree species. *Front. For. Glob. Change* <https://doi.org/10.3389/ffgc.2020.00025> (2020).
- Leigh, A. et al. Do thick leaves avoid thermal damage in critically low wind speeds? *New Phytol.* **194**, 477–487 (2012).
- Perez, T. M. & Feeley, K. J. Photosynthetic heat tolerances and extreme leaf temperatures. *Funct. Ecol.* **34**, 2236–2245 (2020).
- Pacifici, M. et al. Assessing species vulnerability to climate change. *Nat. Clim. Change* **5**, 215–224 (2015).
- Foden, W. B. et al. Climate change vulnerability assessment of species. *WIREs Clim. Change* **10**, e551 (2019).
- Batchuluun, B., Dandarmaa, B. & Munstermann, L. E. The nesting ecology of social wasps (Hymenoptera: Vespidae: Vespinae and Polistinae) in northern Mongolia. *Mong. J. Biol. Sci.* **16**, 49–58 (2018).
- Abaimov, A. P. in *Permafrost Ecosystems: Siberian Larch Forests* (eds Osawa, A. et al.) Chapter 2 (Springer, 2010).
- Schulte, L. et al. Larix species range dynamics in Siberia since the Last Glacial captured from sedimentary ancient DNA. *Commun. Biol.* **5**, 570 (2022).
- Mamet, S. D., Brown, C. D., Trant, A. J. & Laroque, C. P. Shifting global Larix distributions: northern expansion and southern retraction as species respond to changing climate. *J. Biogeogr.* **46**, 30–44 (2019).
- Dulamsuren, C., Hauck, M., Khishigiargal, M., Leuschner, H. H. & Leuschner, C. Diverging climate trends in Mongolian taiga forests influence growth and regeneration of *Larix sibirica*. *Oecologia* **163**, 1091–1102 (2010).
- White, A. J. & Critchley, C. Rapid light curves: a new fluorescence method to assess the state of the photosynthetic apparatus. *Photosynth. Res.* **59**, 63–72 (1999).
- Pontius, J. & Hallett, R. Comprehensive methods for earlier detection and monitoring of forest decline. *For. Sci.* **60**, 1156–1163 (2014).
- Wilcoxon, F. Individual comparisons by ranking methods. *Biometrics Bull.* **1**, 80–83 (1945).
- Ritchie, R. J. Fitting light saturation curves measured using modulated fluorometry. *Photosynth. Res.* **96**, 201–215 (2008).
- Demmig-Adams, B. & Adams Iii, W. W. Photoprotection in an ecological context: the remarkable complexity of thermal energy dissipation. *New Phytol.* **172**, 11–21 (2006).
- Sonti, N. F., Hallett, R. A., Griffin, K. L., Trammell, T. L. E. & Sullivan, J. H. Chlorophyll fluorescence parameters, leaf traits and foliar chemistry of white oak and red maple trees in urban forest patches. *Tree Physiol.* **41**, 269–279 (2020).
- O'Leary, M. H. Carbon Isotopes in Photosynthesis: Fractionation techniques may reveal new aspects of carbon dynamics in plants. *Bioscience* **38**, 328–336 (1988).
- Prieto, I., Querejeta, J. I., Segrestin, J., Volaire, F. & Roumet, C. Leaf carbon and oxygen isotopes are coordinated with the leaf economics spectrum in Mediterranean rangeland species. *Funct. Ecol.* **32**, 612–625 (2018).
- Scheidegger, Y., Saurer, M., Bahn, M. & Siegwolf, R. Linking stable oxygen and carbon isotopes with stomatal conductance and photosynthetic capacity: a conceptual model. *Oecologia* **125**, 350–357 (2000).
- Craine, J. M. et al. Ecological interpretations of nitrogen isotope ratios of terrestrial plants and soils. *Plant Soil* **396**, 1–26 (2015).
- Xu, S., Sardans, J., Zhang, J. & Peñuelas, J. Variations in foliar carbon:nitrogen and nitrogen:phosphorus ratios under global change: a meta-analysis of experimental field studies. *Sci. Rep.* **10**, 12156 (2020).
- Sparks, J. P. & Ehleringer, J. R. Leaf carbon isotope discrimination and nitrogen content for riparian trees along elevational transects. *Oecologia* **109**, 362–367 (1997).
- Craine, J. M. et al. Global patterns of foliar nitrogen isotopes and their relationships with climate, mycorrhizal fungi, foliar nutrient concentrations, and nitrogen availability. *New Phytol.* **183**, 980–992 (2009).
- Evans, R. D. Physiological mechanisms influencing plant nitrogen isotope composition. *Trends Plant. Sci.* **6**, 121–126 (2001).
- Santarius, K. A. Seasonal changes in plant membrane stability as evidenced by the heat sensitivity of chloroplast membrane reactions. *Zeitschrift für Pflanzenphysiologie* **73**, 448–451 (1974).

63. Zhu, L. et al. Plasticity of photosynthetic heat tolerance in plants adapted to thermally contrasting biomes. *Plant Cell Environ.* **41**, 1251–1262 (2018).
64. Perez, T. M., Socha, A., Tserelj, O. & Feeley, K. J. Photosystem II heat tolerances characterize thermal generalists and the upper limit of carbon assimilation. *Plant Cell Environ.* **44**, 2321–2330 (2021).
65. Berry, J. A. & Bjorkman, O. Photosynthetic response and adaptation to temperature in higher plants. *Ann. Rev. Plant Physiol.* **31**, 491–543 (1980).
66. Slot, M. et al. Leaf heat tolerance of 147 tropical forest species varies with elevation and leaf functional traits, but not with phylogeny. *Plant Cell Environ.* **44**, 2414–2427 (2021).
67. Daas, C., Montpied, P., Hanchi, B. & Dreyer, E. Responses of photosynthesis to high temperatures in oak saplings assessed by chlorophyll-a fluorescence: inter-specific diversity and temperature-induced plasticity. *Ann. For. Sci.* **65**, 305 (2008).
68. Drake, J. E. et al. Trees tolerate an extreme heatwave via sustained transpirational cooling and increased leaf thermal tolerance. *Global Change Biol.* **24**, 2390–2402 (2018).
69. Grossman, J. J. Phenological physiology: seasonal patterns of plant stress tolerance in a changing climate. *New Phytol.* **237**, 1508–1524 (2023).
70. Still, C. J. et al. No evidence of canopy-scale leaf thermoregulation to cool leaves below air temperature across a range of forest ecosystems. *Proc. Natl Acad. Sci. USA* **119**, e2205682119 (2022).
71. Koyama, K. & Takemoto, S. Morning reduction of photosynthetic capacity before midday depression. *Sci. Rep.* **4**, 4389 (2014).
72. Špunda, V. et al. Diurnal dynamics of photosynthetic parameters of Norway spruce trees cultivated under ambient and elevated CO<sub>2</sub>: the reasons of midday depression in CO<sub>2</sub> assimilation. *Plant Sci.* **168**, 1371–1381 (2005).
73. Roessler, P. G. & Monson, R. K. Midday depression in net photosynthesis and stomatal conductance in *Yucca glauca*. *Oecologia* **67**, 380–387 (1985).
74. Perez, T. M. & Feeley, K. J. Increasing humidity threatens tropical rainforests. *Front. Ecol. Evol.* <https://doi.org/10.3389/fevo.2018.00068> (2018).
75. Hersbach, H. et al. ERA5 hourly data on single levels from 1979 to present. Copernicus Climate Change Service (C3S) Climate Data Store (CDS). <https://doi.org/10.24381/cds.adbb2d47> (2018).
76. Jin, M. & Dickinson, R. E. Land surface skin temperature climatology: benefitting from the strengths of satellite observations. *Environ. Res. Lett.* **5**, 044004 (2010).
77. Le Quéré, C. et al. Global carbon budget 2018. *Earth Syst. Sci. Data* **10**, 2141–2194 (2018).
78. Friedlingstein, P. et al. Uncertainties in CMIP5 climate projections due to carbon cycle feedbacks. *J. Clim.* **27**, 511–526 (2014).
79. Chylek, P. et al. Annual mean arctic amplification 1970–2020: observed and simulated by CMIP6 climate models. *Geophys. Res. Lett.* **49**, e2022GL099371 (2022).
80. Anderegg, W. R. L., Trugman, A. T., Badgley, G., Konings, A. G. & Shaw, J. Divergent forest sensitivity to repeated extreme droughts. *Nat. Clim. Change* **10**, 1091–1095 (2020).
81. Curtis, E. M., Gollan, J., Murray, B. R. & Leigh, A. Native microhabitats better predict tolerance to warming than latitudinal macro-climatic variables in arid-zone plants. *J. Biogeogr.* **43**, 1156–1165 (2016).
82. Hytteborn, H., Maslov, A., Nazimova, O. & Rysin, L. Boreal forests of Eurasia. in *Coniferous Forests* (ed. Andersson, F. A.) Chapter 2 (Elsevier Science, 2005).
83. Park, G. E. et al. Morphological characteristics and water-use efficiency of Siberian Elm trees (*Ulmus pumila* L.) within arid regions of Northeast Asia. *Forests* **7**, 280 (2016).
84. Dulamsuren, C., Hauck, M. & Leuschner, C. Recent drought stress leads to growth reductions in *Larix sibirica* in the western Khentey, Mongolia. *Glob. Change Biol.* **16**, 3024–3035 (2010).
85. Seidl, R. et al. Forest disturbances under climate change. *Nat. Clim. Change* **7**, 395–402 (2017).
86. Li, W. et al. Reassessment of growth-climate relations indicates the potential for decline across Eurasian boreal larch forests. *Nat. Commun.* **14**, 3358 (2023).
87. Thrasher, B. et al. NASA global daily downscaled projections, CMIP6. *Sci. Data* **9**, 262 (2022).
88. Koven, C. D. Boreal carbon loss due to poleward shift in low-carbon ecosystems. *Nat. Geosci.* **6**, 452–456 (2013).
89. Rogers, A. et al. A roadmap for improving the representation of photosynthesis in Earth system models. *New Phytol.* **213**, 22–42 (2017).
90. Braghiere, R. K. et al. Tipping point in North American Arctic-Boreal carbon sink persists in new generation Earth system models despite reduced uncertainty. *Environ. Res. Lett.* **18**, 025008 (2023).
91. Gardner, W. R. M. & Burentogtokh, J. Mobile domiciles of the Eurasian steppe: archaeological evidence of possible dwelling space during the early iron age. *J. Field Archaeol.* **43**, 345–361 (2018).
92. Rascher, U., Liebig, M. & Lüttge, U. Evaluation of instant light-response curves of chlorophyll fluorescence parameters obtained with a portable chlorophyll fluorometer on site in the field. *Plant Cell Environ.* **23**, 1397–1405 (2000).
93. Harris, I., Osborn, T. J., Jones, P. & Lister, D. Version 4 of the CRU TS monthly high-resolution gridded multivariate climate dataset. *Sci. Data* **7**, 109 (2020).
94. Morice, C. P. et al. An updated assessment of near-surface temperature change from 1850: the HadCRUT5 data set. *J. Geophys. Res. Atmos.* **126**, e2019JD032361 (2021).
95. O'Neill, B. C. et al. The scenario model intercomparison project (ScenarioMIP) for CMIP6. *Geosci. Model Dev.* **9**, 3461–3482 (2016).
96. Potapov, P., Hansen, M. C., Stehman, S. V., Loveland, T. R. & Pittman, K. Combining MODIS and Landsat imagery to estimate and map boreal forest cover loss. *Remote Sens. Environ.* **112**, 3708–3719 (2008).
97. Olson, D. M. et al. Terrestrial ecoregions of the World: a new map of life on Earth: a new global map of terrestrial ecoregions provides an innovative tool for conserving biodiversity. *Bioscience* **51**, 933–938 (2001).
98. Riahi, K. et al. The shared socioeconomic pathways and their energy, land use, and greenhouse gas emissions implications: an overview. *Glob. Environ. Change* **42**, 153–168 (2017).
99. Nobel, P. S. *Physicochemical & Environmental Plant Physiology* (Academic Press, 1999).

## Acknowledgements

The authors are grateful to William Honeychurch and the participants at the 2019 Tarvagtai Field Camp for assistance with logistics and fieldwork. The authors thank Benjamin Harlow at Stable Isotope Core Laboratory, Washington State University, for processing the foliar chemistry and folia isotope samples. The study was funded by the NOAA Climate and Global Change Postdoctoral Fellowship Programme administered by UCAR-CPAESS under award #NA18NWS4620043B, European Union Horizon 2020 Marie Skłodowska-Curie grant #101031748, National Science Foundation Office of Polar Programmes (NSF-OPP) award #1737788, and NUM grant #P2019-3634. A.M.V.-C. and L.A.H. acknowledge NSF Partnership for International Research and Education (PEER) award #OISE-1743738. N.K.D. and C.L. acknowledge NSF Arctic Social Science award #2112463.

## Author contributions

M.P.R. and K.L.G. designed the field component of the study and analyzed the field data with contributions from N.K.D., T.S.M., L.A.-H., B.N., B.S., L.O., M.R.-C., J.B. and W.R.M.G. M.P.R., A.M.V.-C. and B.I.C. designed earth system model experiments. Fieldwork was performed by M.P.R., L.O., J.B. and W.R.M.G. M.P.R. performed all experiments and drafted the manuscript. All authors (including N.P., R.D.D. and C.L.) read, edited, contributed to and approved the final version of the manuscript.

## Competing interests

The authors declare no competing interests.

## Additional information

**Supplementary information** The online version contains supplementary material available at <https://doi.org/10.1038/s43247-023-00910-6>.

**Correspondence** and requests for materials should be addressed to Mukund Palat Rao.

**Peer review information** *Communications Earth & Environment* thanks Christoph Leuschner and the other, anonymous, reviewer(s) for their contribution to the peer review of this work. Primary Handling Editor: Joe Aslin. A peer review file is available.

**Reprints and permission information** is available at <http://www.nature.com/reprints>

**Publisher's note** Springer Nature remains neutral with regard to jurisdictional claims in published maps and institutional affiliations.



**Open Access** This article is licensed under a Creative Commons Attribution 4.0 International License, which permits use, sharing, adaptation, distribution and reproduction in any medium or format, as long as you give appropriate credit to the original author(s) and the source, provide a link to the Creative Commons licence, and indicate if changes were made. The images or other third party material in this article are included in the article's Creative Commons licence, unless indicated otherwise in a credit line to the material. If material is not included in the article's Creative Commons licence and your intended use is not permitted by statutory regulation or exceeds the permitted use, you will need to obtain permission directly from the copyright holder. To view a copy of this licence, visit <http://creativecommons.org/licenses/by/4.0/>.

© The Author(s) 2023